Front. Earth Sci. 2014, 8(4): 610–624
DOI 10.1007/s11707-014-0455-6

RESEARCH ARTICLE

Retrievals of aerosol optical depth and total column ozone from Ultraviolet Multifilter Rotating Shadowband Radiometer measurements based on an optimal estimation technique

Chaoshun LIU (✉)[1,2], Maosi CHEN[2], Runhe SHI[1,2], Wei GAO[1,2]

1 Key Laboratory of Geographic Information Science, Ministry of Education, East China Normal University, Shanghai 200062, China
2 USDA UV-B Monitoring and Research Program, Natural Resource Ecology Laboratory, Colorado State University, Fort Collins CO 80523, USA

Abstract A Bayesian optimal estimation (OE) retrieval technique was used to retreive aerosol optical depth (AOD), aerosol single scattering albedo (SSA), and an asymmetry factor (g) at seven ultraviolet wavelengths, along with total column ozone (TOC), from the measurements of the UltraViolet Multifilter Rotating Shadowband Radiometer (UV-MFRSR) deployed at the Southern Great Plains (SGP) site during March through November in 2009. The OE technique specifies appropriate error covariance matrices and optimizes a forward model (Tropospheric ultraviolet radiative transfer model, TUV), and thus provides a supplemental method for use across the network of the Department of Agriculture UV-B Monitoring and Research Program (USDA UVMRP) for the retrieval of aerosol properties and TOC with reasonable accuracy in the UV spectral range under various atmospheric conditions. In order to assess the accuracy of the OE technique, we compared the AOD retreivals from this method with those from Beer's Law and the AErosol RObotic Network (AERONET) AOD product. We also examine the OE retrieved TOC in comparison with the TOC from the U.S. Department of Agriculture UV-B Monitoring and Research Program (USDA UVMRP) and the Ozone Monitoring Instrument (OMI) satellite data. The scatterplots of the estimated AOD from the OE method agree well with those derived from Beer's law and the collocated AERONET AOD product, showing high values of correlation coefficients, generally 0.98 and 0.99, and large slopes, ranging from 0.95 to 1.0, as well as small offsets, less than 0.02 especially at 368 nm. The comparison of TOC retrievals also indicates the promising accuracy of the OE method in that the standard deviations of the difference between the OE derived TOC and other TOC products are about 5 to 6 Dobson Units (DU). Validation of the OE retrievals on these selected dates suggested that the OE technique has its merits and can serve as a supplemental tool in further analyzing UVMRP data.

Keywords optimal estimation, aerosol optical depth, total column ozone, Ultraviolet Multifilter Rotating Shadowband Radiometer (UV-MFRSR), Aerosol Robotic Network (AERONET), Tropospheric ultraviolet radiative transfer model (TUV)

1 Introduction

Ultraviolet (UV) radiation, invisible to the human eye, is part of the electromagnetic radiation emitted by the sun. Although UV radiation constitutes less than 7% of solar radiation in the vacuum that reaches the Earth's surface (Caldwell, 1971), it has great impact on human health (such as causing skin cancers and the diseases related to eyes and the immune system), and affects animals, marine organisms, and plants, as well as crop yields (Rötter and van de Geijn, 1999; Kakani et al., 2003; Gallagher and Lee, 2006). It also contributes to climate change and environmental stresses via regulating the emission rates of several atmospheric trace gases, including ozone, carbonyl sulfide, methane, methyl bromide, and dimethyl sulfide (Zepp et al., 2007). On the other hand, ozone is known as the most important UV radiation absorber in the atmosphere, and it can effectively reduce the UV radiation reaching the Earth's surface. As such, the decrease of ozone concentration in the atmosphere will inevitably lead to the increase of UV radiation at the terrestrial surface. Thus, absorption by the atmospheric ozone column is a primary factor for UV radiation extinction.

Received November 1, 2013; accepted February 28, 2014

E-mail: csliu@re.ecnu.edu.cn

Ozone depletion had been observed since the late 1970s (Prather and Watson, 1990; Solomon, 1999). So far, numerous investigations have been made to monitor ozone concentration in the atmosphere and analyze the temporal and spatial variations of the total ozone column (TOC) by using ground-based measurements, satellite remote sensing, and model simulations for ozone layer protection. Several instruments, such as the Total Ozone Mapping Spectrometer (TOMS), the Ozone Monitoring Instrument (OMI), the Global Ozone Monitoring Experiment (GOME-2), and the Infrared Atmospheric Sounding Interferometer (IASI) have been installed on satellite platforms. They can provide daily TOC observations globally and/or ozone profile information at multiple spatial and temporal resolutions, facilitating a better understanding of the geographical distribution and temporal variability of ozone on the global scale (Stolarski et al., 1991; Antón et al., 2009, 2011). Reliable ground-based ozone measurements, such as Brewer spectrophotometers, Dobson spectrophotometers (Balis et al., 2007), and the Ultraviolet Multifilter Rotating Shadowband Radiometer (UV-MFRSR) (Bigelow et al., 1998) can be utilized to assess the quality and accuracy of satellite TOC observations. UV-MFRSR TOC measurements are in good agreement with the Brewer and Dobson instrument counterparts under all sky conditions, and UV-MFRSR is superior in having a long-term unattended deployment and routine measurement of TOC due to automatic operation, relatively low cost, and high accuracy (Slusser et al., 1999; Gao et al., 2001).

Atmospheric aerosols also affect UV radiation by scattering and absorbing effects. Aerosols and clouds in the troposphere attenuate UV radiation to such an extent that the effect of stratospheric ozone is obscured (Bordewijk et al., 1995). Analysis of ground-based UV measurements can improve the understanding of the aerosol attenuation that is of importance for reducing UV irradiance retrieval errors in satellite remote sensing observations. Moreover, aerosol optical properties, such as aerosol optical depth (AOD), single-scatter albedo (SSA), and the asymmetry parameter (g), are also required as input variables in order to improve the output accuracy of UV radiative transfer models (Ricchiazzi et al., 1998; McComiskey et al., 2008). These optical properties can help us understand UV radiation and its interaction with aerosols better.

Many useful methods have been adopted in order to determine the above critical parameters (or parameters of interest). No matter what method is used, the calibration coefficient(s) of the UV-MFRSR that makes the radiation observed at the Earth's surface comparable to that measured at the top of the atmosphere should be obtained somehow before the retrieval of AOD. The classic Langley regression method has been routinely applied to provide such calibration coefficients in situ during an AOD stable period (usually morning). Then, the total optical depth(s) can be derived according to Beer's Law (Herman et al., 1975; Holben et al., 1998; Slusser et al., 2000). In particular, the assumption of AOD stability is critical to the Langley method. Moreover, cloudy measurements should be removed before the linear regression is performed. Lee et al. (2010) modified the standard Langley method by acquiring the maximum value composite (MVC) of the largest irradiance (voltage) values during a window of several days within small airmass intervals. The comparison of the derived AOD using this method with the interpolated AOD from the AErosol RObotic Network (AERONET) CIMEL sun photometers (Holben et al., 1998) shows that the relative errors of AOD for 5, 7, and 10 days are all about 20%, while 7.5% for 30 days (Lee et al., 2010). Ratios of diffuse-to-direct irradiances, independent of the instruments' absolute calibration uncertainties, have been used to determine AOD and SSA in the UV range (Petters et al., 2003; Meloni et al., 2006; Medina et al., 2012). In order to address the situation when the Beer's Law is not valid but radiation transfer modeling is necessary, the Bayesian optimal estimation technique was developed for simultaneous retrievals of AOD, SSA, and g, at seven wavelengths, as well as daily TOC (Goering et al., 2005; Taylor et al., 2008). Slusser et al. (1999) and Gao et al. (2001) presented an alternative TOC retrieval technique specifically designed for the UV-MFRSR direct beams. They assumed that Beer's Law is applicable, and that the total optical depth difference between two double-channel pairs tends to cancel out the influence of Rayleigh scattering and aerosol effects, leaving the ozone optical depth as the only significant component in the equation.

The purpose of this paper is to present the applicability and accuracy of the optimal estimation technique — the Tropospheric UltraViolet radiative transfer model (TUV v4.2) as the forward model — in retrieving AOD, SSA, g, and TOC from UV-MFRSR measurements under cloudless skies. A detailed description of the measurements, the OE retrieval algorithm, and the accuracy assessment of the TUV model are given in section 2. In section 3 analyses of the AOD and TOC retrievals of the OE method are presented and compared to other independent measurements. The final results are summarized in section 4.

2 Measurements and methodology

2.1 Site information and instruments description

The UV-MFRSR (Fig. 1) in this study is operated by the U. S. Department of Agriculture (USDA) UV-B Monitoring and Research Program (UVMRP) and manufactured by Yankee Environmental Systems. It is deployed at the top of a low hill south of the central facility of the Southern Great

Plains (SGP) site of the US Department of Energy (DOE) (97.49°W, 36.60°N, 317 m above sea level) on a cattle farm, or ranch. The UV-MFRSR was installed at the site which was established by the DOE's Atmospheric Radiation Measurement Program (ARM) in February 1999. The local topography is very flat and the land use is mostly for agriculture. The main land cover is winter wheat and pasture. The SGP is the largest and most extensive climate research field and one of the best equipped, well-designed, and well-maintained instrumentation sites in the world (Inamdar et al., 2008). Many scientists are using the information obtained from the SGP site in order to improve the knowledge of cloud, aerosol, water vapor, trace gases, and radiation characterizations (Stokes and Schwartz, 1994; Morcrette, 2002).

Fig. 1 The UV-MFRSR deployed at US Department of Energy ARM/SGP/CART site.

The UV-MFRSR measures the total and diffuse solar irradiance and computes the direct irradiance at 300, 305, 311, 317, 325, 332, and 368 nm with a nominal 2 nm FWHM for each narrowband in the UV-B and UV-A regions (Bigelow et al., 1998). Figure 2 shows some examples for optical depths of atmospheric constituents which affect the UV-MFRSR spectral region, and seven UV-MFRSR filter functions are displayed, representing the relative response of individual channels as a function of wavelength. Total and diffuse irradiance are recorded every 20 seconds from which the corresponding direct normal component is derived. The data are averaged and stored at 3-minute intervals. In order to convert the voltage readings to physically meaningful quantities, various data processing procedures must be employed. After an offset correction and a cosine response correction, a calibration factor must be applied to yield irradiances in the unit of watts per square meter per nanometer. The calibration parameters determined before deployment can shift dramatically and quickly in the field, which means frequent calibrations are necessary in order to produce reliable radiation measurements. There are two methods to get the calibration factor. The first one is the lamp calibration that was supplied by the manufacturer at the time of instrument acquisition. Periodic lamp calibration throughout the year is necessary because the extraterrestrial signal will slowly change due to filter drift (Augustine et al., 2003; Chen et al., 2013), which is relatively inconvenient and expensive for operational implementation. Due to the lack of updated information from lamp-calibration, another method that has been used widely to derive calibration factors is the in situ Langley method. It should always be considered more accurate than the lamp-calibrated method when there are enough Langley events under clear days. For each UV-MFRSR channel (λ), the Langley calibration method can be used to convert measured voltage to irradiances by

$$I_\lambda = V_\lambda \times I_{0,\lambda}/V_{0,\lambda}, \tag{1}$$

where, I_λ is the band-pass direct normal irradiance reaching the Earth's surface at channel λ; V_λ is the measured voltage by UV-MFRSR; I_0 is the band-pass extraterrestrial solar irradiance. It is calculated for each channel of the instrument in each deployment period by using the most recent filter function to weight the Solar Spectral Irradiance Monitor (SUSIM) spectrum; $V_{0,\lambda}$ is the corresponding voltage intercept calibrated by Langley method.

Calibration by the Langley method makes use of the Lambert-Beer Law in extrapolating the measured direct beam to zero air mass where the incident irradiance is equal to the extra-terrestrial value. Solar direct beam irradiance through the Earth's atmosphere can be described by the Lambert-Beer Law:

$$I_\lambda = R^2 I_{0,\lambda} \exp(-\tau_{\mathrm{Total},\lambda} \cdot m), \tag{2}$$

where, R is the Earth-Sun distance in astronomical units (AU); m is the air mass factor which is essentially equal to the inverse of the cosine of the solar zenith angle (SZA) for small to moderate values; and $\tau_{\mathrm{Total},\lambda}$ is the total optical depth at channel λ; and the other notations retain the same meaning as before. The components of $\tau_{\mathrm{Total},\lambda}$ include AOD τ_a, Rayleigh optical thickness τ_{R} , and ozone absorption optical thickness $\tau_{\mathrm{O_3}}$:

$$\tau_{\mathrm{Total},\lambda} = \tau_a + \tau_{\mathrm{R}} + \tau_{\mathrm{O_3}}. \tag{3}$$

Substituting Eq. (1) into Eq. (2), rearranging the terms, and taking the logarithm of both sides, Eq. (2) becomes:

$$\ln V_\lambda = \ln V_{0,\lambda} + \ln R^2 - \tau_{\mathrm{Total},\lambda} \cdot m. \tag{4}$$

A plot of $\ln(V_\lambda)$ against air mass factor m will yield a straight line with the intercept at zero airmass, which is equal to $\ln V_{0,\lambda} + \ln R^2$, and with the slope of the line, which is the average total optical depth. Given the determination of daily $V_{0,\lambda}$ coefficients, AOD of an individual channel under cloud free days can be calculated from Eq. (3) by subtracting contributions due to absorption by atmospheric gases (in this case, ozone, $\tau_{\mathrm{O_3}}$) and Rayleigh scattering (τ_{R}, parameterized by (Bodhaine et al., 1999)):

$$\tau_a = -\frac{1}{m}\ln\left(\frac{1}{R^2}\frac{V_\lambda}{V_{0,\lambda}}\right) - \tau_R - \tau_{O_3}. \quad (5)$$

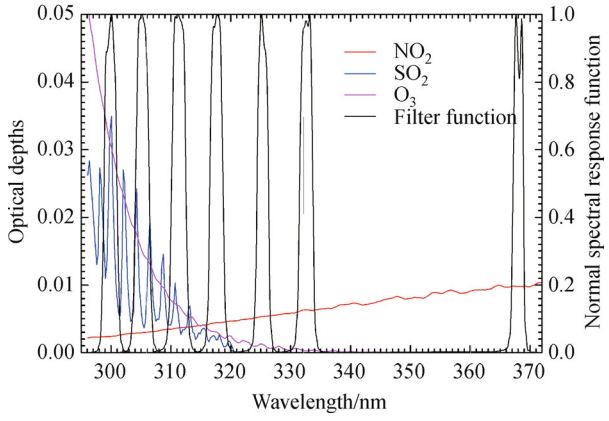

Fig. 2 The filter function (dash line) of UV-MFRSR at the SGP site from 12 December 2006, and typical optical depths of atmospheric constituents calculated by TUV4.2 in the UV-MFRSR spectral region: NO_2 (0.7 DU column amount, red line); SO_2 (1 DU column amount, blue line); and O_3 (300 DU column amount, magenta line).

2.2 Methodology

The conventional Langley calibration has been deemed invalid or impractical under highly variable atmospheric conditions, which are very common in the world. Additionally, attenuation due to Rayleigh scattering from atmospheric gases and absorption by ozone needed to be determined before calculating AOD from Rayleigh, ozone, and total optical depth. Performing calibrations under less than ideal atmospheric conditions can lead to incorrect estimations of I_0 and errors in AOD retrievals (Lee et al., 2010). A retrieval algorithm based on Bayesian optimal estimation (OE) has been developed and refined in order to simultaneously determine AOD and SSA at seven wavelengths in the UV range, as well as TOC and a wavelength-independent asymmetry factor (g), using direct and diffuse irradiances measured with the UV-MFRSR (Goering et al., 2005; Taylor et al., 2008). Following Goering et al. (2005), the relationship between the physical properties of the atmosphere and the measured radiometric quantities can be generalized using the following expression:

$$\boldsymbol{y} = F(\boldsymbol{x},\boldsymbol{b}) + \varepsilon, \quad (6)$$

where, $\boldsymbol{y}$ is the measurements vector (corresponding direct normal and diffuse horizontal irradiance measured by the UV-MFRSR in this context); while the state vector $\boldsymbol{x}$ is defined for the retrieval paramaters (consists of TOC and g, in addition to AOD and SSA at the center wavelength of each passband); F is the forward model describing radiative transfer through the atmosphere (the Tropospheric Ultraviolet and Visible model, TUV4.2, was chosen in this case); $\boldsymbol{b}$ represents a vector of parameters not included in the state vector, but assumed to be known as TUV model inputs; ε is an all-encompassing error term accounting for the measurement error and measurement noise as well as for the forward model error and uncertainties in the forward model parameter assumptions.

Proceeding with the formulation of the optimal estimation framework through the use of Bayes's theorem, a cost function can be defined as follows (Goering et al., 2005; Taylor et al., 2008):

$$\boldsymbol{\Phi} = (\boldsymbol{y}-F(\hat{\boldsymbol{x}}))^{\mathrm{T}}\boldsymbol{S}_y^{-1}(\boldsymbol{y}-F(\hat{\boldsymbol{x}})) + (\hat{\boldsymbol{x}}-\boldsymbol{x}_a)^{\mathrm{T}}\boldsymbol{S}_a^{-1}(\hat{\boldsymbol{x}}-\boldsymbol{x}_a). \quad (7)$$

The maximum probability solution of $\boldsymbol{x}$ is solved when the gradient of $\boldsymbol{\Phi}$ with respect to $\boldsymbol{x}$ has reached a minimum. Linearizing the forward model about some base state $\hat{\boldsymbol{x}}_{i-1}$, the solution can be found in an iterative manner using Newton's method (Rodgers, 2000), given by:

$$\hat{\boldsymbol{x}} = \hat{\boldsymbol{x}}_{i-1} + \hat{\boldsymbol{S}}\left[\boldsymbol{K}^{\mathrm{T}}\boldsymbol{S}_y^{-1}(\boldsymbol{y}-F(\hat{\boldsymbol{x}}_{i-1}))\boldsymbol{S}_a^{-1}(\boldsymbol{x}_a-\hat{\boldsymbol{x}}_{i-1})\right], \quad (8)$$

where

$$\hat{\boldsymbol{S}} = (\boldsymbol{S}_a^{-1} + \boldsymbol{K}^{\mathrm{T}}\boldsymbol{S}_y^{-1}\boldsymbol{K})^{-1}, \quad (9)$$

determines the associated retrieval covariance matrix. Here, $\hat{\boldsymbol{x}}$ represents the estimated values of the unknown state parameters; $\boldsymbol{x}_a$ is the a priori state vector representing the best guess of the retrieval parameters prior to measurement; $\boldsymbol{K}$ is the Jacobian or weighting function matrix representing the sensitivity of the linearized forward model to a change in the state parameter; diagonal elements of $\boldsymbol{S}_y$ and $\boldsymbol{S}_a$ provide the error covariance from both the measurement and model error covariance and the a priori error covariance of the state, respectively, while off-diagonal elements indicate uncertainty correlations between vector elements.

The retrieval a larger number of parameters than the number of available measurements is a key feature of the OE approach because of the additional information provided by the a priori state vector, and the ability to impose correlations on AOD and SSA as an exponential function of wavelength via the off-diagonal elements of the a priori error covariance matrix, $\boldsymbol{S_a}$. This reduces the number of independent variables that need to be retrieved and provides more realistic estimates of the state parameters. Appropriate a priori error covariance matrices assignment and forward model optimization are critical to the operational implementation of the Bayesian optimal estimation algorithm described above. The a priori error covariance matrix, $\boldsymbol{S}_a$, is a 16-by-16 matrix. The diagonal elements of the $\boldsymbol{S}_a$ matrix are assumed to follow a Gaussian

distribution and are defined by assigning a priori values of and standard deviations (σ) for each parameter (TOC, AOD, SSA, g) . We assign correlation among the off-diagonal elements using exponential decay with increasing wavelength (i.e., $\sigma_{i,j} = \sqrt{\sigma_i \sigma_j} \exp\left(-(\lambda_i - \lambda_j)^2 / 8^2\right)$. Referring to the reported values in the previous literature, a priori information used for optimal estimation retrievals at the SGP site can be summarized as follows: 0.80 for AOD with a standard deviation of 0.5, 0.85 for SSA with a standard deviation of 0.1, 0.7 for the asymmetry factor (g) with a standard deviation of 0.15, and 295 DU for TOC with a standard deviation of 44, or dynamic values for TOC with a standard deviation of 2% of daily TOC that are based on the daily mean TOC when the UV-MFRSR TOC data set via the direct sun technique (Gao et al., 2001) are available. Taylor et al. (2008) summarized that the uncertainties in all seven passbands accounted for the $\boldsymbol{S}_y$ error covariance matrix from measurements and the forward model by using sensitivity testing. For the purposes of this study, the default values of channel error were given in percentages for calculating direct (diffuse) irradiances due to uncertainties in model variables, with values of 5.11(5.56) at 300 nm, 5.03(5.25) at 305 nm, 4.89 (5.11) at 311 nm, 4.82(5.11) at 317 nm, 4.68(4.97) at 325 nm, 4.54(4.83) at 332 nm, and 4.01(4.37) at 368 nm, respectively.

Clouds can attenuate the direct solar irradiance that contributes to the production of more diffuse solar radiation. Consequently, it is necessary to perform cloud screening in order to remove cloud contaminated data, avoiding large biases in aerosol retrievals due to cloud cover effects. Current methods for cloud screening often apply empirical threshold values to the standard deviation of measurements or the ratio between the direct and diffuse amount (Alexandrov et al., 2004). The results are highly dependent upon the thresholds in which clouds significantly vary across different observation sites and the thresholds need to be further determined. The more detailed discussion of cloud screening could be found in Chen et al. (2013). For simplicity, the cloud screening procedure in this study was accomplished by using the AERONET Level 2.0 quality assured data as criteria, which were pre- and post-field calibrated, automatically cloud cleared, manually inspected (see AERONET web page, Version 2 AOD Descriptions), and collocated with SGP UV-MFRSR. Cloud free was assumed within the UV-MFRSR measurement periods if the collocated AERONET CIMEL sun photometer had successfully retrieved the AOD product.

2.3 The Forward Model

A tropospheric ultraviolet radiative transfer model, TUV4.2, was chosen as the forward model for the retrieval of the corresponding AOD, SSA, TOC, and g values, due to its successful application to these parameter in other studies (Petters et al., 2003; Balis et al., 2004; Goering et al., 2005; Taylor et al., 2008; Perrin et al., 2005; Meloni et al., 2006; Medina et al., 2012). In order to ensure that this forward model is capable of simulating UV-MFRSR measurements, separate model runs were performed to check the individual simulation of bands with inputs as summarized in Table 1 for 1 to 5 November, 2009 at the SGP site. The values of AOD in seven passbands were calculated by interpolating the retrieved AOD of AERONET. The amount of TOC was derived from the UV-MFRSR TOC data set via the Direct-Sun technique (Gao et al., 2001). The asymmetry factor (g) was also based on the AERONET inversion data product. A surface albedo of 5% and SSA of 0.85 at all wavelengths were used as a priori in this check and retrival within this context. The TUV was run with the 8-stream Discrete Ordinate Method based on inputs in Table 1 and other parameters were fixed in the forward model in order to simulate the direct and diffuse irradiances, each of which was weighted by the spectral response functions of the UV-MFRSR instrument and integrated over the entire spectrum.

The calculated irradiances from the TUV model were compared with those obtained from the UV-MFRSR instrument. Figure 3 shows very good agreement between the observed and simulated irradiance components at the SGP site, from 1 to 5 November, 2009. The averaged differences between observed and simulated results for direct normal, diffuse horizontal, and total horizontal irradiances are summarized in Table 2. The RMSE and median difference over the time series did not exceed 5% at 317 nm, 325 nm, 332 nm, and 368 nm, which are less affected by O_3, NO_2, and SO_2 atmospheric gases, while those values are slightly greater than or near 5% at 300 nm,

Table 1 Summary of TUV inputs for November 1 to 5, 2009 at SGP site

Date	AOD							SSA all λ	TOC /DU	g	Albedo
	300 nm	305 nm	311 nm	317 nm	325 nm	332 nm	368 nm				
2009-11-1	0.0514	0.0499	0.0486	0.0472	0.0456	0.044	0.038	0.85	260	0.70	0.05
2009-11-2	0.1080	0.1050	0.1020	0.0993	0.0962	0.093	0.081	0.85	248	0.65	0.05
2009-11-3	0.1629	0.1582	0.1534	0.1587	0.1584	0.153	0.143	0.85	249	0.60	0.05
2009-11-4	0.1682	0.1632	0.1582	0.1533	0.1477	0.142	0.121	0.85	251	0.60	0.05
2009-11-5	0.1844	0.1780	0.1715	0.1652	0.1582	0.151	0.125	0.85	250	0.60	0.05

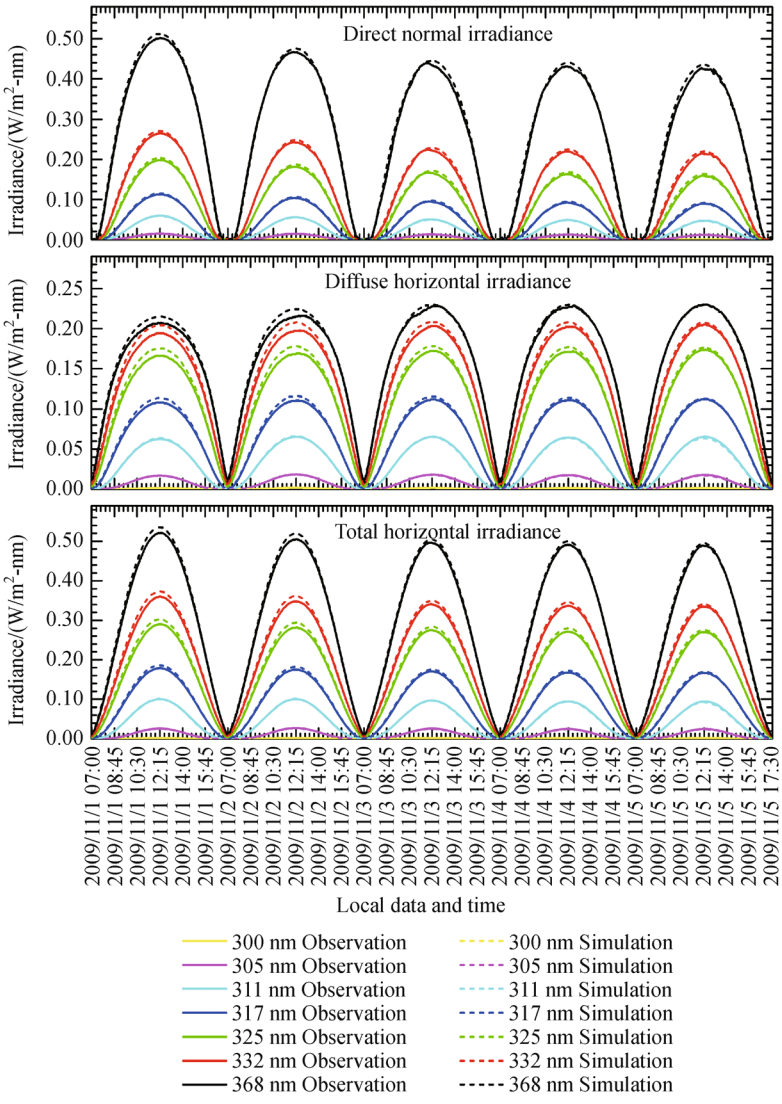

Fig. 3 Comparison of observed and simulated direct normal (top), diffuse horizontal (middle), and total horizontal (bottom) irradiances at SGP site, from 1 to 5 November, 2009. Solid lines represent observations and dashed lines represent simulations.

305 nm, and 311 nm. On the other hand, the magnitude of shorter wavelength irradiances is much less than that of longer wavelengths, which also accounts for the big relative difference. Overall, the agreement of all channels in the UV range was better than 8%. This comparison suggests that UV radiation exposure can be computed with strong confidence for clear sky conditions by using the TUV model if the appropriate atmospheric data are available, including TOC data, surface albedo, molecular density profiles, and aerosol optical properties.

There are several radiative transfer solvers (n-stream Discrete Ordinate Method, n-DOM) within the TUV code such as 4, 8, and 32 streams, and the 2-stream Delta-Eddington (Δ-ED) approximation (Stamnes et al., 1988). The fewer streams involved with the DOM selected in the forward model, the faster the model runs, such that it may yield large irradiance differences. Several numerical simulations were performed in order to investigate the percent differences between the 4-DOM and the 32-DOM approximation used in the forward model with different AOD, SSA, SZA, TOC, and wavelengths. The values of TOC and SZA are 270 DU, 295 DU, 330 DU and 25º, 45º, and 65º, respectively. The AOD increases from 0.1 to 2.0 with a step of 0.1, while the SSA ranges from 0.65 to 0.95 with an increment of 0.3. The range and increment of each variable used provides a realistic and broad cover of the parameters in the SPG site. The 4-DOM calculation is about 30 times faster than that of 32-DOM. These simulations show that the TOC has little or no effect over the entire AOD-SSA domain space for all seven wavelengths and SZA. So, the differences between these factors are only presented in Fig. 4 with 295 DU TOC. The columns in Fig. 4 indicate differences for different SZA values, and the rows for different wavelengths. For SZA

Table 2 Averaged differences of comparison between observed and simulated irradiances at the SGP site from 1 to 5 November, 2009

Band/nm	Direct normal irradiance		Diffuse horizontal irradiance		Total horizontal irradiance	
	Absolute differences RMSE/Median /($W \cdot m^{-2} \cdot nm^{-1}$)	Relative differences RMSE/ Median /%	Absolute differences RMSE/ Median /($W \cdot m^{-2} \cdot nm^{-1}$)	Relative differences RMSE/ Median /%	Absolute differences RMSE/ Median /($W \cdot m^{-2} \cdot nm^{-1}$)	Relative differences RMSE/ Median /%
300	1.830E–5/ 1.912E–5	5.043/ 5.042	4.184E–5/ 5.120E–5	3.494/ 8.435	5.281E–5/ 5.954E–5	3.974/ 7.221
305	1.130E–4/ 1.360E–4	4.499/ –1.748	1.530E–4/ 1.770E–4	4.771/ –1.434	1.950E–4/ 2.400E–4	4.957/ –1.666
311	3.290E–4/ 4.740E–4	7.864/ –0.952	4.200E–4/ 6.600E–4	2.012/ –0.095	4.750E–4/ 7.820E–4	2.122/ –0.411
317	1.176E–3/ 1.820E–3	4.477/ 2.934	1.238E–3/ 2.580E–3	1.539/ 3.282	1.852E–3/ 3.566E–3	1.709/ 3.032
325	2.262E–3/ 4.040E–3	4.328/ 3.329	1.958E–3/ 4.940E–3	1.347/ 3.820	3.133E–3/ 6.980E–3	1.531/ 3.479
332	2.529E–3/ 4.500E–3	3.950/ 2.541	2.126E–3/ 5.400E–3	1.222/ 3.517	3.450E–3/ 7.600E–3	1.475/ 3.034
368	4.553E–3/ 8.600E–3	3.051/ 2.259	1.899E–3/ 3.400E–3	1.063/ 1.691	3.556E–3/ 7.080E–3	1.197/ 1.936

25º (left column) the differences do not exceed 1% for all wavelengths in the entire AOD-SSA domain. The error gradually increases with increasing SZA. Particularly for SZA at 65º (right column), the biases become more dependent on AOD, while still slightly dependent on SSA. At 300 nm (the upper-right of Fig. 4), the differences range from 1% to 7.5%, whereas the biases are smaller, ranging from about –2.8% to 2% over the domain (the right-lower of the figures). It is important to note that the 4-DOM scheme provides operational performance that compromises the speed and the accuracy of TUV model, and thus has been adopted for use in the Bayesian optimal estimation retrieval algorithm.

3 Results and discussion

After using the method described in section 2.2 for cloud screening, retrievals for UV-MFRSR measurements collected at the SGP site during March to November, 2009 were performed based on a Bayesian optimal estimation (OE) algorithm using the a priori state vector and variances summarized above. Figure 5 illustrates the temporal variation of AOD (Figs. 5(a) and 5(c)) and SSA (Figs. 5 (b) and 5(d)) for all of the UV-MFRSR channels on 15 March and 27 September, 2009, respectively. In order to evaluate the performance of the retrieval more comprehensively, several widely-used independent results were selected in this context for comparison.

As described in section 2.1, a Langley calibration analysis was attempted for each morning and afternoon period corresponding to the time of a selected air mass factor range. Ideally, by assuming stability of AOD during the morning and afternoon periods, the Langley calibrations of the UV-MFRSR data would produce two intercept values (one for morning, another for afternoon) for each channel during each day of instrument operation (see Fig. 6 (a), which is the plot of Ln (mV) versus air mass factor (1/m) in this notation). A voltage intercept value (V_0) is needed, which converts measured voltages to irradiances using the Langley calibration method and is subsequently associated with aerosol optical depths and column ozone retrievals. It is accordingly taken as the intercept of the line at air mass factor 0 while the slope of the line is the average optical depth. Since the V_0 represents the voltage that would be measured by the instrument if it were placed at the top of the atmosphere, the intercept would be constant ideally. However, the intercept points vary greatly and distribute sparsely at more turbid atmospheric conditions from site to site. Figure 6(b) illustrates the difference between the retrieval AOD values from the UV-MFRSR 368 nm channel using the AM and PM calibrated V_0 values on 30 May, 2009.

The voltage intercept values are 1,568.93 mV and 1,708.08 mV derived from AM and PM data, respectively, resulting in a maximum relative difference between the two time series of AOD in Fig. 6(b), potentially, of more than 30%. In order to make the comparisons more credible, both of two time series (AM and PM) AOD values are used for comparison if they are available. Moreover, there is often no Langley voltage intercept value (V_0) generated when there are few Langley events under turbid atmospheric conditions. To overcome this limitation of the traditional Langley calibration method (called old Langley calibration in following), the USDA UVMRP developed the latest in situ calibration procedure (described as the new Langley calibration) in order to generate the voltage intercept values, which are the time smoothed version of

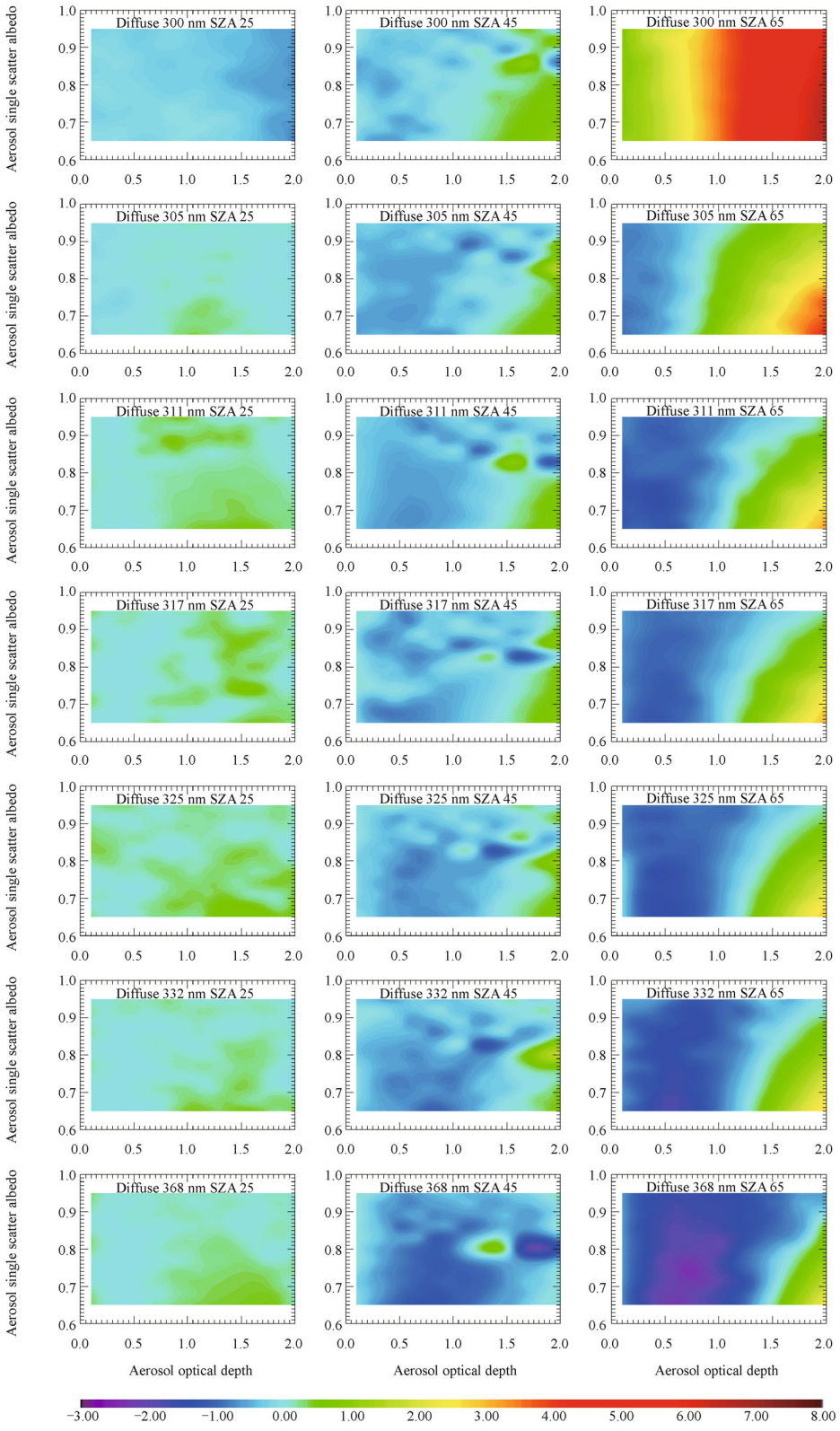

Fig. 4 Percent differences of simulated diffuse irradiance between the 4-DOM and the 32-DOM used in TUV with TOC = 295 DU.

the old Langley calibration V_0 values. Unlike smoothing that merely uses the target time series, the new Langley calibration method also considers the Lamp calibrated V_0 values as a guide. These new Langley calibration products

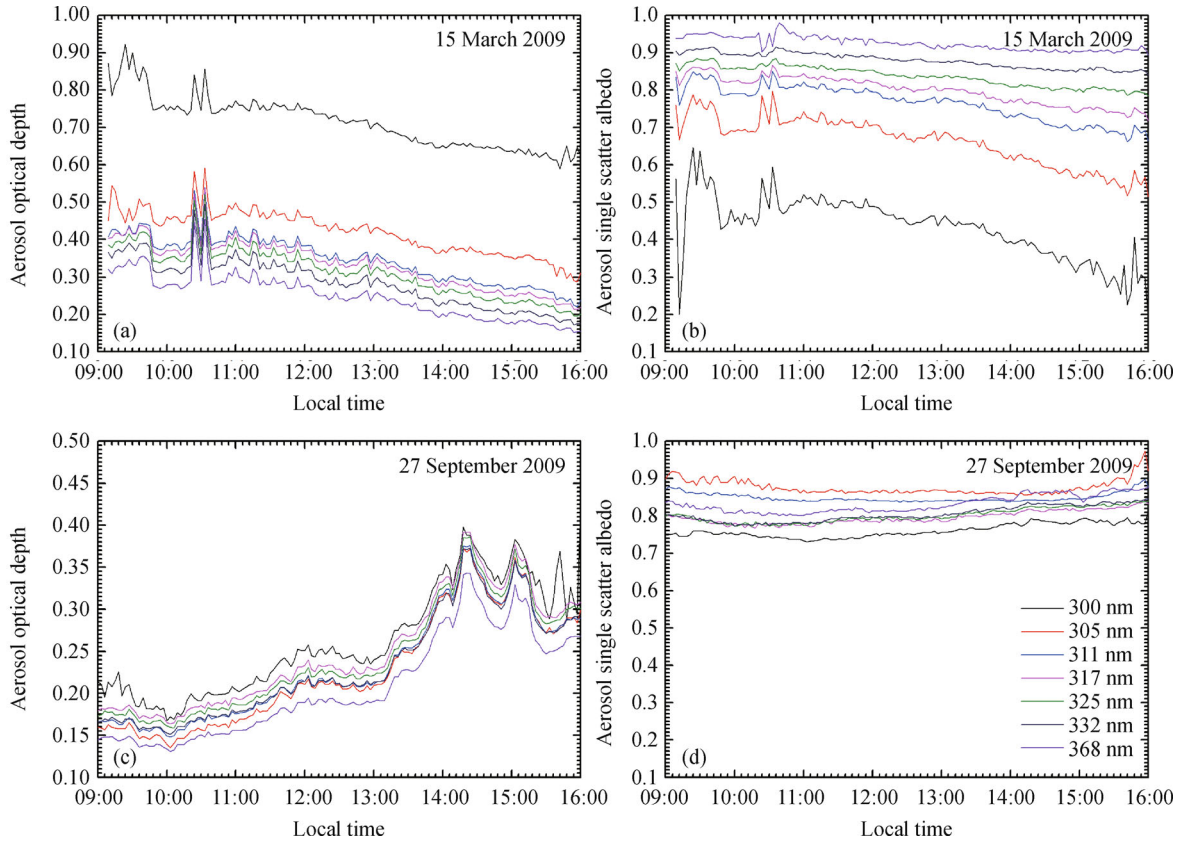

Fig. 5 Time series of retrieval aerosol optical depth (left) and single scatter albedo (right) for the UV-MFRSR seven passbands on 15 March and 27 September, 2009.

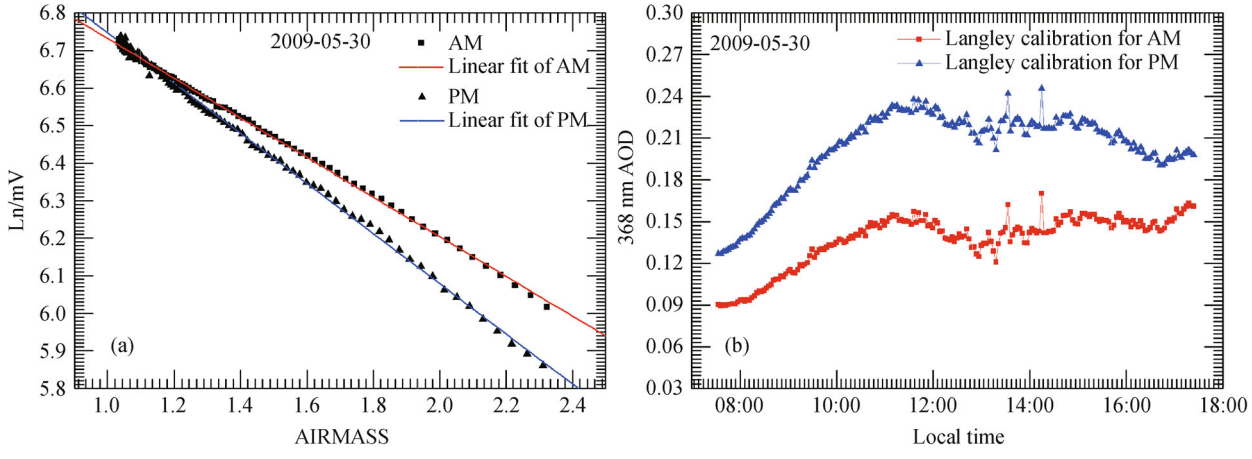

Fig. 6 Langley plot (a) for the AM and PM data and retrieval AOD (b) of the UV-MFRSR 368 nm channel obtained on 30 May 2009 at the SGP site.

can be downloaded from the USDA UVMRP website. Any detailed questions regarding the latest in situ Langley calibration procedure should be directed to the UVMRP. Both of the AOD results derived from the two Langley regression methods described above are compared with the OE AOD results here in order to evaluate the performance of the OE retrieval.

Additional AOD values used for comparison in this study were obtained from the Level 2.0 products of the AERONET CIMEL Sun photometer, which was collocated with the UV-MFRSR instrument at the Cart site (longitude = 97.486°W, latitude = 36.607°N, elevation =

318 m). All AERONET data can be found at http://aeronet.gsfc.nasa.gov/. The AOD values derived from the AERONET CIMEL sun photometer at the channels of 340 nm, 380 nm, 440 nm, 500 nm, 675 nm, 870 nm, and 1,020 nm are not consistent with those retrieved from the UV-MFRSR, whose spectral passbands were 300 nm, 305 nm, 311 nm, 317 nm, 325 nm, 332 nm, and 368 nm, respectively. According to Krotkov et al. (2005), AERONET discrete spectral measurements could be interpolated or extrapolated to any given wavelength within the UV-MFRSR spectral bandbass (Krotkov et al., 2005). In this research, only two wavelengths of UV-MFRSR, 332 nm and 368 nm, which are both less affected by O_3, NO_2, and SO_2 atmospheric gases (Medina et al., 2012) (Fig. 2), were selected for AOD comparison with those interpolated from AERONET data. The AERONET AOD measurements at 340 nm, 380 nm, 440 nm, and 500 nm were extrapolated to 332 nm and interpolated to 368nm of the UV-MFRSR wavelengths using linear fit in ln(AOD) versus ln (wavelength) space by minimizing the Chi-square error statistic. The typical differences between the extrapolation or interpolation methods at these channels were less than 0.005 (Krotkov et al., 2005). For a better comparison, the OE AOD results of the UV-MFRSR were averaged into the bins with the same intervals as the AERONET level 2.0 AOD product, considering that AERONET uses direct-Sun irradiance measurements at about 15 minute intervals to measure aerosol optical depth, while the UV-MFRSR instrument has intervals of 3 minutes. The standard deviations of the UV-MFRSR AOD values retrieved by the OE algorithm within the AERONET AOD measurement intervals have been calculated and presented as error bars in Fig. 7.

From March to November, 2009 UV-MFRSR data for 19 days which were cloud free but under highly variable atmospheric conditions were selected for analysis with the OE retrieval algorithm and the Langley methods. Figure 7 shows scatterplots comparing OE AOD with AOD derived from the old Langley calibration (top panel) and new Langley calibration (middle panel), as well as the AERONET AOD (bottom panel). The AOD ranges from about 0.08 to 1.58 which almost covers all of the AOD variations during clear sky at the research site. Although it might be expected that the retrieval will perform poorly as the AOD increases, the scatters are much closer to the 1:1 line when the values of AOD are greater than 1.0 in Fig. 7. This indicates that the OE retrievals are more reliable under high atmospheric turbidity conditions. The left panel shows the results for the 332 nm channel while the right one for 368 nm. In general, the linear fit lines on the right side (the slope values closer to 1 with large values of R^2 and small intercepts) are much closer to the 1:1 line than those on the left panels. Additionally, the standard deviations of the bias differences (SDBD) as well as the mean absolute percentage differences (MAPD) for 368 nm, summarized in Table 3, are smaller than those for 332 nm, all indicating that retrieval results are better at the longer wavelength (i.e., 368 nm). These differences are mainly due to the strong attenuation of radiation caused by O_3, NO_2, and SO_2 atmospheric gases at the short wavelengths.

The top panel of Fig. 7 shows that AODs estimated from UV-MFRSR data by using the old Langley calibration have an overestimation compared to the OE AODs. The agreement between the three inter-comparisons is the worst, as shown by the lowest values of squared correlation coefficient (R^2= 0.6791, 0.8228) with large slopes (0.7343, 0.7760) and intercepts (0.0881, 0.0280), and also by the largest absolute values of mean bias difference (MBD =–0.0138, –0.0286), MAPD (32.06%, 22.31%), and SDBD (0.0892, 0.0646) for 332 nm and 368 nm, respectively. There is no guarantee, as described above, that AOD retrievals by using the old Langley calibration will perform well under extremely hazy atmospheric conditions or dramatic AOD variations, hence, the data for these circumstances were also selected in this study.

The middle panel of Fig. 7 shows excellent agreement between OE AODs and AODs using the new Langley calibration method, with R^2 (0.9911, 0.9958) of the linear regression, SDBD (0.0256, 0.0156), and MAPD (7.86%, 7.69%) for 332 nm and 368 nm, respectively. The OE retrievals of 368 nm have a weak overestimation compared to AODs derived from the new Langley method, as shown by the slope of 1.0007 and intercept of –0.0146. Conversely, for 332 nm, the OE AOD values are slightly underestimated, with a slope of 0.9648 and intercept of 0.0158.

The values of R^2 between the OE AODs and AERONET AODs for both 332 nm and 368 nm are both greater than 0.96, indicating that they have a good linear correlation, shown at the bottom panels of Fig. 7. Compared with AERONET AODs, the OE AODs for 368 nm have less underestimation than those of 332 nm, shown by the contrary values of slope (0.9513, 0.0158) and intercept (0.8090, 0.0425). The smallest values of MAPD (7.16%, 5.81%) and SDBD (0.0216, 0.0144) are found among the three inter-comparisons for 332 nm and 368 nm, respectively. They suggest that the AODs estimated from UV-MFRSR data for 332 nm and 368 nm using the OE method agree quite well with those from the AERONET CIMEL Sun photometer retrievals. The difference in calibration procedures (CIMEL is calibrated by comparison with the master instrument at the NASA Goddard Space Flight Center (Alexandrov et al., 2008), while the UV-MFRSR is calibrated from the data) and/or the extrapolation and interpolation of AERONET AOD spectral measurements to UV-MFRSR wavelengths may also account for the disagreement (or discrepancy) between the OE AODs and AERONET AODs. Overall, the difference in AODs derived from OE and AERONET is acceptable and can be considered to be a result of different operational

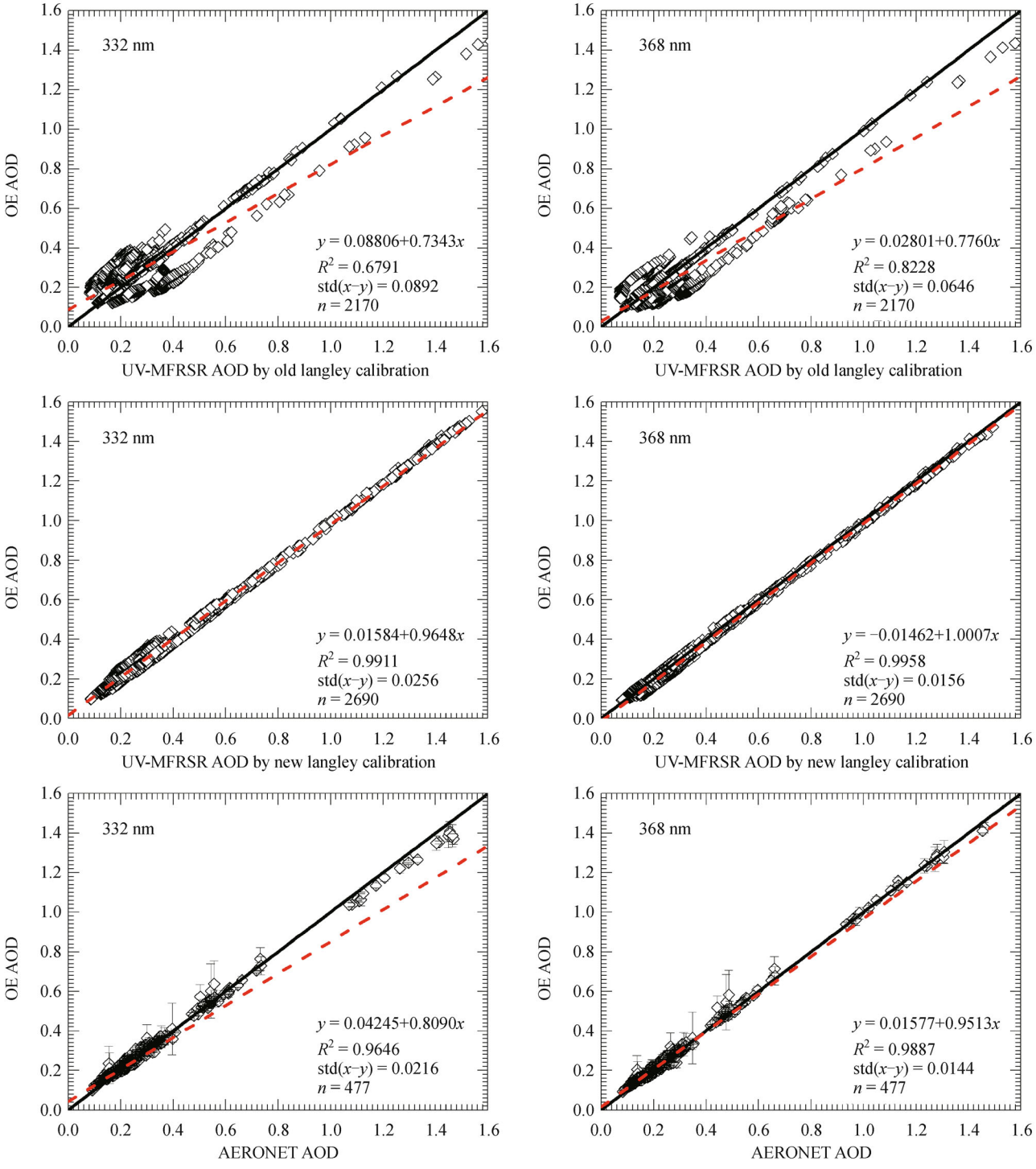

Fig. 7 Comparison of OE AOD between the UV-MFRSR data retrievals derived from old (top panel) and new (middle panel) Langley algorithms as well as AERONET AOD (level 2.0 data, bottom panel, error bars correspond to standard deviation) during March to November, 2009 (19 days). The black solid line is the 1:1 line and the red dash line is the linear regression on the set of data points based on the least-square method with statistics summarized at the lower right of each plot.

algorithms in retrieving the AOD values across the USDA UVMRP network.

Table 3 summarizes the AOD comparison statistics between the results of the OE, the Old Langley calibration, the New Langley calibration, and the AERONET methods at the 332 nm and 368 nm wavelengths as further evidence of the precision with which the results agreed. The statistics in Table 3 indicate that the OE algorithm can

converge on a solution, and thus provides a reasonable estimation of AOD.

The TOC comparison data used in this paper are available through the USDA UVMRP website using the Direct-Sun method (Gao et al., 2001), and the Goddard Earth Sciences Data and Information Services Center (GESDISC) derived from the Ozone Monitoring Instrument (OMI) onboard the Earth Observing System (EOS) Aura satellite using the OMI-TOMS and the OMI-DOAS algorithms, respectively. The TOC derived by OE were averaged to daily intervals because only daily mean values of observations are available for comparison. Figure 8 compares the daily total ozone column retrieved by OE, Direct-Sun, OMI-TOMS, and the OMI-DOAS algorithms, respectively. The error bars represent standard deviations from the mean values, reflecting the daily variations for TOC.

The daily results for TOC using OE range from 266.34 DU to 339.66 DU with a median of 295.02 DU and mean of 300.46 DU. The median value of the differences between the OE and Direct-Sun is only 0.61 DU (i.e., about 0.2% of typical ozone column amount) indicating that the OE ozone retrievals appear to be practically unbiased. The standard deviation between them was 5.46 DU (about 2%, relative to the typical value of 300 DU). The maximum daily TOC results using OE range from

Table 3 Summary of comparison statistics in AOD retrieved using Optimal Estimation versus different methods

Channel		OE vs Old langley	OE vs New langley	OE vs AERONET
332 nm	Slope	0.7343	0.9648	0.8090
	Intercept	0.0881	0.0158	0.0425
	R^2	0.6791	0.9911	0.9646
	MBD	–0.0138	0.0025	–0.0080
	SDBD	0.0892	0.0256	0.0216
	MAPD	32.06%	7.86%	7.16%
368 nm	Slope	0.7760	1.0007	0.9513
	Intercept	0.0280	–0.0146	0.0158
	R^2	0.8228	0.9958	0.9887
	MBD	–0.0286	–0.0144	–0.0061
	SDBD	0.0646	0.0156	0.0144
	MAPD	22.31%	7.69%	5.81%

Note: R^2 is the squared correlation coefficient; MBD is mean bias difference denoted as $\frac{1}{n}\sum_1^n(y_i-x_i)$; SDBD is standard deviation of the bias difference expressed as $\sqrt{\sum_1^n[(y_i-x_i)-MBD]^2/(n-1)}$; MAPD is mean absolute percentage difference calculated as $\frac{1}{n}\sum_1^n(|y_i-x_i|/x_i)\times 100\%$.

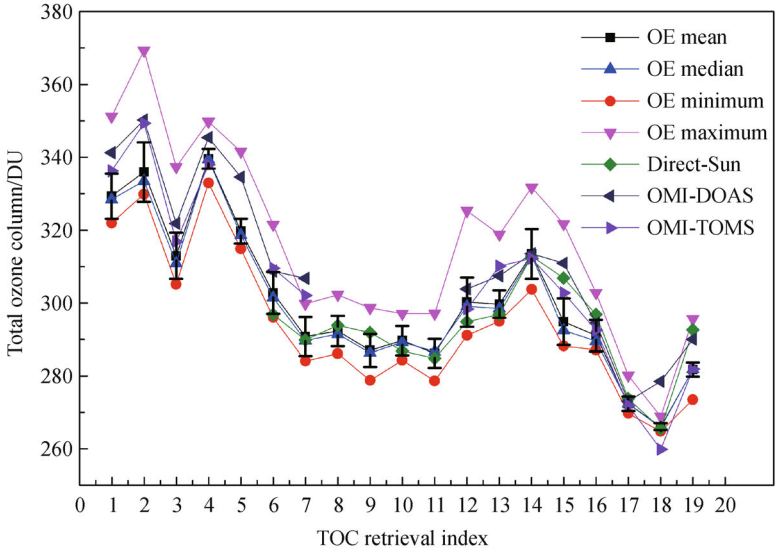

Fig. 8 Comparison of daily total ozone column retrieved by OE, Direct-Sun, OMI-TOMS, and the OMI-DOAS algorithms, respectively (error bars represent standard deviation).

269.08 DU to 369.26 DU with a median of 318.94 DU, while the minimum ranges from 265.02 DU to 333 DU with a median of 288.34 DU. The maximum-minimum domain almost covers all of the ranges of TOC variation from OE, Direct-Sun, OMI-TOMS, and OMI-DOAS. The median and standard deviation of TOC differences between OE and OMI-DOAS are –8.23 DU and 5.49 DU, respectively, while those values are –2.68 DU and 5.89DU for OE versus OMI-TOMS.

Among these three inter-comparison datasets, the largest bias (16.08 DU) was identified with OMI-DOAS measurements. Overall, the inter-comparison results confirm that the OE retrieved values all agree well with those data drawn from the Direct-Sun, OMI-TOMS, and OMI-DOAS algorithms, respectively, with about 5 to 6 DU daily standard deviation of differences between them. The difference in averaging/sampling between satellite-based and ground-based measurements and uncertainties of the measurements both contribute to the disagreement. In addition, the accurate retrieval of TOC is critical to the retrieval of aerosol properties at the shorter wavelength channels where the attenuation of radiation is very sensitive to ozone absorption in the Huggins bands.

Retrieved values of SSA and g were also acquired during these days. However, there were no independent measurements of SSA and g available for direct comparison at this site and time period, so more efforts will be needed for a more complete validation of this technique.

4 Conclusions

A retrieval algorithm based on Bayesian optimal estimation (OE) is described in this work and has been used to simultaneously determine AOD and SSA at seven wavelengths in the UV range, as well as TOC and a wavelength-independent asymmetry factor (g). This algorithm employs direct and diffuse irradiances measured with the UV-MFRSR instrument deployed at the Southern Great Plains (SGP) site during March to November, 2009. Cloud screening based on AERONET data was performed before the OE retrievals in order to remove cloud contaminated data which produces large biases in AOD retrievals. Several widely-used results from independent sources were selected for comparison in order to evaluate the performance of the retrievals. Results show that the OE technique tends to provide accurate and useful results. The AOD values for 332 nm and 368 nm derived by the OE method were compared with Langley-derived and collocated AERONET AODs. It shows that the OE AOD data agree well with the AOD values derived from the new Langley calibration and AERONET, especially for 368 nm, where correlation coefficients are on the order of 0.98–0.99, the slopes range from 0.95 to 1.0, and offsets are less than 0.02. Additionally, the comparison of the results from OE TOC with results for the TOC derived by Direct-Sun, OMI-TOMS, and OMI-DOAS algorithms also confirms that the OE method produces realistic estimates, with about a 5 to 6 DU difference for the daily standard deviation .

The forward model experiment shows that UV radiation exposure can be computed with confidence for clear sky conditions by using a TUV model if the appropriate atmospheric data such as TOC data, surface albedo, molecular density profiles, and aerosol optical properties are available. The 4-DOM scheme of the forward model, TUV4.2, provides operational skills which compromise the speed and the accuracy of TUV model. This scheme thus has been adopted for use in a Bayesian optimal estimation retrieval algorithm. Appropriate a priori error covariance matrices assignment and model optimization are critical for providing operational performance at the cost of the speed and the accuracy of OE retrievals. The OE algorithm can allow us to retrieve more parameters than measurements along with the additional constraints of an exponential function of wavelength correlation between AOD and SSA, as well as more information provided by the a priori state vector.

Overall, the OE approach provides a supplemental way to perform AOD and TOC retrievals efficiently in a wider range of atmospheric conditions than the traditional Langley technique. It generates the most useful information during more turbid conditions that routinely exist at most UVMRP sites. Although more data is needed for conclusive results, this investigation establishes reasonable confidence in the application of the OE technique across the USDA UVMRP network to retrievals of aerosol properties in the UV spectral range and TOC. The realistic values derived from this technique can help to improve our understanding of air pollution, UV radiation, climate change, and satellite retrievals validation. It must be pointed out, however, that more studies are required in order to implement the OE algorithm operationally. An automated cloud screening algorithm for UV-MFRSR data should be developed primarily for more efficient usage. Moreover, future research is needed for a complete validation of the OE technique. Changing the a priori covariances and/or using radiative transfer approximation with more accurate versions during different atmospheric conditions before operational application across the UVMRP network could contribute to the validation of the OE technique.

Acknowledgements This work was supported by the National Natural Science Foundation of China (Grant No. 41101037), the National Basic Research Program of China (No. 2010CB951603), USDA NIFA project (2011-34263-30654), the Research Fund for the Doctoral Program of Higher Education (20100076120024), and the Fundamental Research Funds for the Central Universities (East China Normal University). We would also like to thank the PI investigators and their staff for establishing and maintaining the AERONET site used in this investigation.

References

Alexandrov M D, Lacis A A, Carlson B E, Cairns B (2008). Characterization of atmospheric aerosols using MFRSR measurements. J Geophys Res, 113(D8): D08204

Alexandrov M D, Marshak A, Cairns B, Lacis A A, Carlson B E (2004). Automated cloud screening algorithm for MFRSR data. Geophys Res Lett, 31(4): L04118

Antón M, López M, Vilaplana J, Kroon M, McPeters R, Bañón M, Serrano A (2009). Validation of OMI-TOMS and OMI-DOAS total ozone column using five Brewer spectroradiometers at the Iberian peninsula. J Geophys Res, 114(D14): D14307

Antón M, Loyola D, Clerbaux C, López M, Vilaplana J, Banón M, Hadji-Lazaro J, Valks P, Hao N, Zimmer W, Coheur P F, Hurtmans D, Alados-Arboledas L (2011). Validation of the Metop-A total ozone data from GOME-2 and IASI using reference ground-based measurements at the Iberian Peninsula. Remote Sens Environ, 115 (6): 1380–1386

Augustine J A, Cornwall C R, Hodges G B, Long C N, Medina C I, DeLuisi J J (2003). An automated method of MFRSR calibration for aerosol optical depth analysis with application to an Asian dust outbreak over the United States. J Appl Meteorol, 42(2): 266–278

Balis D, Kroon M, Koukouli M, Brinksma E, Labow G, Veefkind J, McPeters R (2007). Validation of Ozone Monitoring Instrument total ozone column measurements using Brewer and Dobson spectrophotometer ground-based observations. J Geophys Res, 112(D24): D24S46

Balis D S, Amiridis V, Zerefos C, Kazantzidis A, Kazadzis S, Bais A F, Meleti C, Gerasopoulos E, Papayannis A, Matthias V, Dier H, Andreae M O (2004). Study of the effect of different type of aerosols on UV-B radiation from measurements during EARLINET. Atmos Chem Phys, 4(2): 307–321

Bigelow D, Slusser J, Beaubien A, Gibson J (1998). The USDA ultraviolet radiation monitoring program. Bull Am Meteorol Soc, 79 (4): 601–615

Bodhaine B A, Wood N B, Dutton E G, Slusser J R (1999). On Rayleigh optical depth calculations. J Atmos Ocean Technol, 16(11): 1854–1861

Bordewijk J, Slaper H, Reinen H, Schlamann E (1995). Total solar radiation and the influence of clouds and aerosols on the biologically effective UV. Geophys Res Lett, 22(16): 2151–2154

Caldwell M M (1971). Solar UV irradiation and the growth and development of higher plants. Photophysiology, 6(13): l–177

Chen M, Davis J, Tang H, Ownby C, and Gao W (2013). The calibration methods for Multi-Filter Rotating Shadowband Radiometer: a review. Front Earth Sci, 7(3): 257–270

Gallagher R P, Lee T K (2006). Adverse effects of ultraviolet radiation: a brief review. Prog Biophys Mol Biol, 92(1): 119–131

Gao W, Slusser J, Gibson J, Scott G, Bigelow D, Kerr J, McArthur B (2001). Direct-sun column ozone retrieval by the ultraviolet multifilter rotating shadow-band radiometer and comparison with those from Brewer and Dobson spectrophotometers. Appl Opt, 40(19): 3149–3155

Goering C D, L'Ecuyer T S, Stephens G L, Slusser J R, Scott G, Davis J, Barnard J C, Madronich S (2005). Simultaneous retrievals of column ozone and aerosol optical properties from direct and diffuse solar irradiance measurements. J Geophys Res, 110(D5): D05204

Herman B, Browning R, De Luisi J (1975). Determination of the effective imaginary term of the complex refractive index of atmospheric dust by remote sensing: the diffuse-direct radiation method. J Atmos Sci, 32(5): 918–925

Holben B, Eck T, Slutsker I, Tanre D, Buis J, Setzer A, Vermote E, Reagan J, Kaufman Y, Nakajima T, Lavenu F, Jankowiak I, Smirnov A (1998). AERONET—A federated instrument network and data archive for aerosol characterization. Remote Sens Environ, 66(1): 1–16

Inamdar A K, French A, Hook S, Vaughan G, Luckett W (2008). Land surface temperature retrieval at high spatial and temporal resolutions over the southwestern United States. J Geophys Res, 113(D7): D07107

Kakani V, Reddy K, Zhao D, Sailaja K (2003). Field crop responses to ultraviolet-B radiation: a review. Agric Meteorol, 120(1): 191–218

Krotkov N, Bhartia P K, Herman J, Slusser J, Labow G, Scott G, Janson G, Eck T F, Holben B (2005). Aerosol ultraviolet absorption experiment (2002 to 2004), part 1: ultraviolet multifilter rotating shadowband radiometer calibration and intercomparison with CIMEL sunphotometers. Opt Eng, 44(4): 041001–041017

Lee K H, Li Z, Cribb M, Liu J, Wang L, Zheng Y, Xia X, Chen H, Li B (2010). Aerosol optical depth measurements in eastern China and a new calibration method. J Geophys Res, 115: D00K11

McComiskey A, Schwartz S E, Schmid B, Guan H, Lewis E R, Ricchiazzi P, Ogren J A (2008). Direct aerosol forcing: calculation from observables and sensitivities to inputs. J Geophys Res, 113(D9): D09202

Medina R, Fitzgerald R M, Min Q (2012). Retrieval of the single scattering albedo in the El Paso-Juarez Airshed using the TUV model and a UV-MFRSR radiometer. Atmos Environ, 46(0): 430–440

Meloni D, Di Sarra A, Pace G, Monteleone F (2006). Aerosol optical properties at Lampedusa (Central Mediterranean). 2. Determination of single scattering albedo at two wavelengths for different aerosol types. Atmos Chem Phys, 6(3): 715–727

Morcrette J J (2002). Assessment of the ECMWF model cloudiness and surface radiation fields at the ARM SGP site. Mon Weather Rev, 130 (2): 257–277

Perrin J M, Thuillier G, Fehrenbach M, Huppert F (2005). A comparison between radiative transfer calculation and pyranometer data gathered at Observatoire de Haute Provence. J Atmos Sol Terr Phys, 67(5): 449–463

Petters J, Saxena V, Slusser J, Wenny B, Madronich S (2003). Aerosol single scattering albedo retrieved from measurements of surface UV irradiance and a radiative transfer model. J Geophys Res, 108(D9): 4288

Prather M J, Watson R T (1990). Stratospheric ozone depletion and future levels of atmospheric chlorine and bromine. Nature, 344 (6268): 729–734

Ricchiazzi P, Yang S, Gautier C, Sowle D (1998). SBDART: a research and teaching software tool for plane-parallel radiative transfer in the Earth's atmosphere. Bull Am Meteorol Soc, 79(10): 2101–2114

Rodgers C D (2000). Inverse Methods for Atmospheric Sounding: Theory and Practice. Hackensack: World Scientific

Rötter R, van de Geijn S (1999). Climate change effects on plant growth,

crop yield and livestock. Clim Change, 43(4): 651–681

Slusser J, Gibson J, Bigelow D, Kolinski D, Disterhoft P, Lantz K, Beaubien A (2000). Langley method of calibrating UV filter radiometers. J Geophys Res, 105(D4): 4841–4849

Slusser J, Gibson J, Bigelow D, Kolinski D, Mou W, Koenig G, Beaubien A (1999). Comparison of column ozone retrievals by use of an UV multifilter rotating shadow-band radiometer with those from Brewer and Dobson spectrophotometers. Appl Opt, 38(9): 1543–1551

Solomon S (1999). Stratospheric ozone depletion: a review of concepts and history. Rev Geophys, 37(3): 275–316

Stamnes K, Tsay S C, WiscombeW, Jayaweera K (1988). Numerically stable algorithm for discrete-ordinate-method radiative transfer in multiple scattering and emitting layered media. Appl Opt, 27(12): 2502–2509

Stokes G M, Schwartz S E (1994). The Atmospheric Radiation Measurement (ARM) Program: programmatic background and design of the cloud and radiation test bed. Bull Am Meteorol Soc, 75(7): 1201–1221

Stolarski R S, Bloomfield P, McPeters R D, Herman J R (1991). Total ozone trends deduced from Nimbus 7 TOMS data. Geophys Res Lett, 18(6): 1015–1018

Taylor T E, L'Ecuyer T S, Slusser J R, Stephens G L, Goering C D (2008). An operational retrieval algorithm for determining aerosol optical properties in the ultraviolet. J Geophys Res, 113(D3): D03201

Zepp R, Erickson Iii D, Paul N, Sulzberger B (2007). Interactive effects of solar UV radiation and climate change on biogeochemical cycling. Photochem Photobiol Sci, 6(3): 286–300